JACS
JOURNAL OF THE AMERICAN CHEMICAL SOCIETY
pubs.acs.org/JACS

Article

Marine Natural Product Chagosendine C Induces Cuproptosis in Colorectal Cancer Cells by Targeting FDX1

Xiaoyu Tao,[▽] Hongru Wang,[▽] Qun Wang,[▽] Chengji Wang,[▽] Chang-Wei Shao, Yang Jin, Dianping Yu, Hongmei Hu, Qing Zhang, Mengting Xu, Xiangxin Geng, Hanchi Xu, Linyang Li, Ruling Shen, Yue-Wei Guo,* Xu-Wen Li,* Sanhong Liu,* and Weidong Zhang*

Cite This: *J. Am. Chem. Soc.* 2025, 147, 37089−37103

Read Online

ACCESS | Metrics & More | Article Recommendations | Supporting Information

ABSTRACT: Colorectal cancer (CRC) treatment is hampered by high recurrence rates and drug resistance. Cuproptosis, a copper-induced cell death mechanism, offers a new therapeutic approach. Here, we identified a marine natural product, chagosendine C (CHC), which kills tumor cells by increasing the intracellular copper ion concentration. CHC and related metal coordination homodimer alkaloids were rapidly synthesized and purified for further pharmacological study. *In vitro*, CHC significantly inhibited HCT116 and RKO CRC cell growth, induced G1 phase arrest and cell death, and overcame oxaliplatin resistance. *In vivo*, CHC suppressed colorectal tumor growth in mice at 40 mg/kg without obvious toxic effects. Mechanistically, CHC induces cuproptosis by targeting FDX1, increasing intracellular copper ions and ROS levels in tumor cells, and leading to cell death. Thus, CHC presents a novel CRC treatment strategy, showing strong antitumor activity and potential to overcome oxaliplatin resistance with promising clinical prospects.

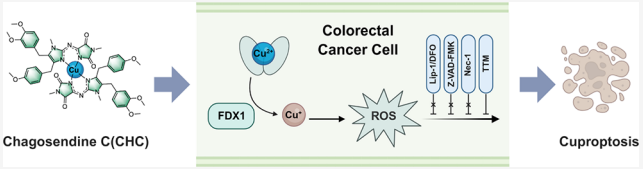

INTRODUCTION

In recent years, the incidence and mortality rates of colorectal cancer (CRC) have steadily increased, making it a major focus of attention in the medical field. Owing to the lack of specific clinical manifestations, approximately 25% of CRC patients are diagnosed at an advanced stage, and approximately 50%−60% of patients experience cancer recurrence or metastasis after treatment, leading to a continuous increase in mortality rates.[1,2] The primary clinical treatment for CRC is surgical resection, but the recurrence rate remains high. Although some progress has been made in the development of current molecular targeted therapies and immunotherapies, their clinical efficacy remains limited due to the development of drug resistance or recurrence.[3,4] These challenges highlight the urgent need for a deeper understanding of the molecular mechanisms underlying CRC progression as well as the identification of new therapeutic targets to develop more effective treatment strategies.

Copper (Cu), an essential trace element, plays a critical role in various biological processes, including mitochondrial respiration, antioxidant defense, and the biosynthesis of biomolecules.[5,6] Its normal function in the body relies on the precise regulation of copper ions. However, an elevated concentration of copper can lead to its accumulation within cells, triggering cytotoxicity and various diseases, including those associated with neurodegenerative disorders[7,8] and tumor progression.[9,10] Cuproptosis, a copper storage disorder, is an example in which excessive copper accumulation causes tissue damage and can even be fatal. Recent studies have shown that copper overload not only induces traditional oxidative stress responses but also triggers cell death through specific mechanisms. In particular, in cuproptosis, copper ions interfere with the lipoic acid-modified components of the tricarboxylic acid (TCA) cycle, forming insoluble aggregates that lead to the accumulation of mitochondrial lipoylated proteins and the loss of function of iron−sulfur (Fe−S) clusters, ultimately resulting in cell death.[11−13] This process is distinct from traditional apoptosis, ferroptosis, or necroptosis, suggesting that copper may play a unique role in cell death mechanisms. In cancer therapy, utilizing this mechanism to develop novel drugs has become a research focus. By promoting copper accumulation within tumor cells, copper toxicity can be enhanced, thereby selectively killing tumor cells.[14−16] Therefore, exploring drugs that can upregulate copper ions will provide new therapeutic strategies for cancers, such as colorectal cancer. These drugs may increase copper bioavailability or directly target copper metabolism pathways, increasing copper concentrations in tumor cells and activating copper-induced cell death pathways. As research into cuproptosis intensifies, combined with modern drug screening technologies and the concept of precision medicine, the

Received: May 11, 2025
Revised: September 8, 2025
Accepted: September 9, 2025
Published: September 22, 2025

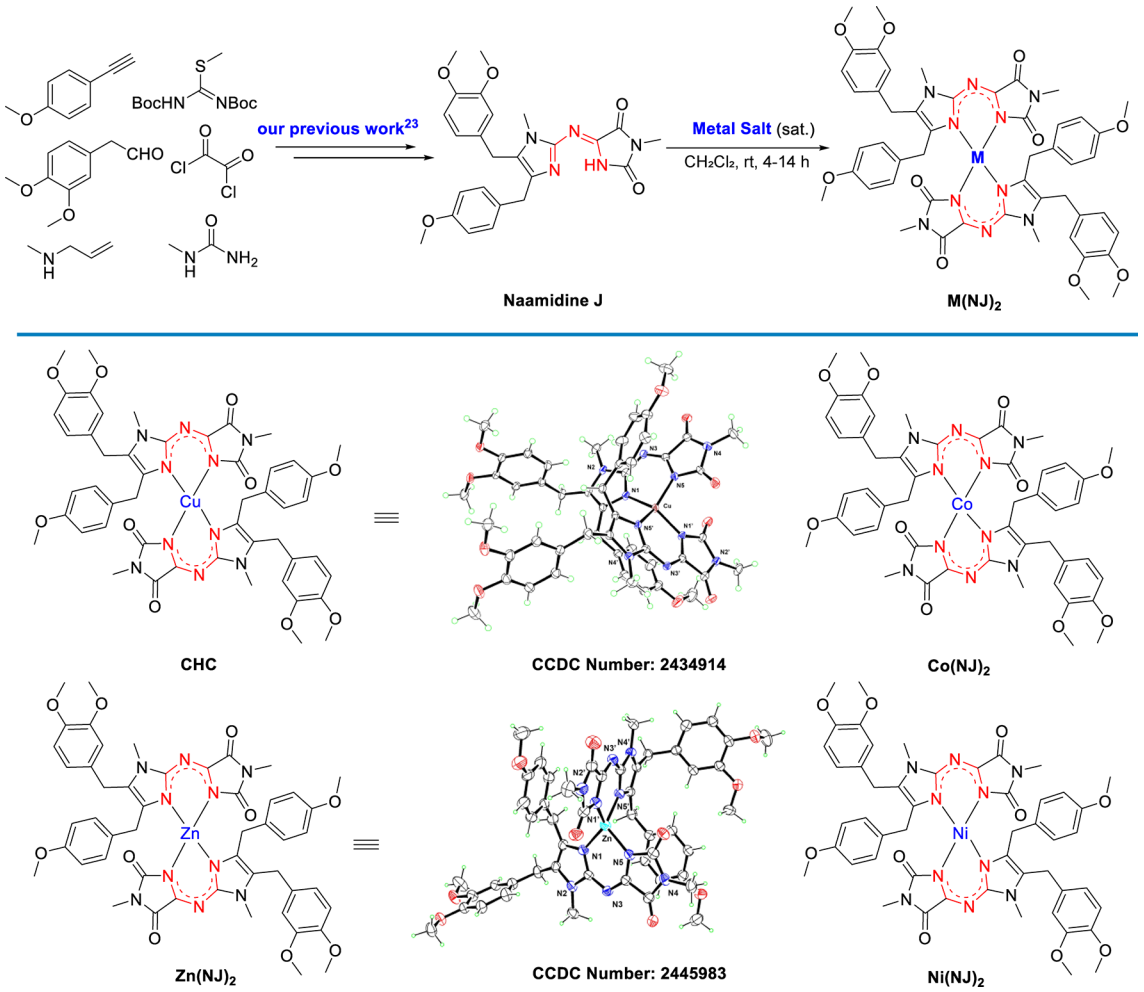

Figure 1. Synthesis of CHC and other related $M(NJ)_2$.

development of copper-metabolism-regulating drugs may become an emerging approach in cancer treatment, offering more treatment options for clinical practice.

Marine natural products, known for their rich diversity and unique structural features, have become important resources for the development of new drugs, particularly in the field of anticancer drug discovery, where they show tremendous potential.[17−20] In this study, we screened a library of marine natural products and identified a compound, chagosendine C (CHC), that has potent antitumor activity in colorectal cancer. CHC is a natural copper coordination homodimer alkaloid.[21] In previous studies, CHC significantly inhibited K562, HepG2, and HeLa cells with IC_{50} values of 0.62, 0.31, and 4.43 μM, respectively. However, it has not been reported in colorectal cancer cells and has potential clinical application value. Our mechanistic findings indicate that CHC induces tumor cell death by targeting FDX1 and increasing the content of Cu^+ in tumor cells, providing a new strategy for the treatment of colorectal cancer.

RESULTS

Structures and Synthesis of CHC and Related Metal Ion Complexes. Marine natural product naamidine J (NJ) has a unique triazacyclo conjugated system that readily chelates with transition metal ions, such as Cu^{2+}, Zn^{2+}, and Ni^{2+}, to form stable organometallic complexes, which led to the generation of the natural products CHC, $Zn(NJ)_2$, and $Ni(NJ)_2$. In order to scale up CHC and related metal coordination homodimer alkaloids, NJ was first synthesized following our previous methods.[22,23] For the metal ion complex synthesis and purification, although the reaction seems to be simple, obtaining the high purity of the complexes and confirming their structures are challenging, since some of them cannot be measured by NMR due to metal effects. For CHC, we dissolved 20.0 mg of NJ in 1 mL of CH_2Cl_2, then added 2 mL of saturated copper sulfate solution. The mixture was stirred at room temperature for 4 h. The organic phase was separated and dried over anhydrous sodium sulfate. The solution was filtered and concentrated under reduced pressure. The residual solid was dissolved in 0.5 mL of ethyl acetate and filtered through an injection filter. Finally, the filtrate was concentrated to dryness to obtain CHC, with HPLC purity greater than 95%. Using the same method, although extending the reaction time, we obtained only crude $Co(NJ)_2$, $Ni(NJ)_2$, and $Zn(NJ)_2$ (TLC detection showed NJ and its metal ion complexes were at the same spot). By optimizing the HPLC method, we obtained three complexes with purity of 96.15% ($Co(NJ)_2$), 98.96% ($Ni(NJ)_2$), and 99.05% ($Zn(NJ)_2$), respectively, for use in bioactivity studies. Notably, $Co(NJ)_2$ was synthesized for the first time and characterized by high-resolution mass spectrometry, providing a library of structurally diverse compounds for chemobiological studies of metal-dependent cell death pathways. Finally, we performed single-

https://doi.org/10.1021/jacs.5c07917
J. Am. Chem. Soc. 2025, 147, 37089−37103

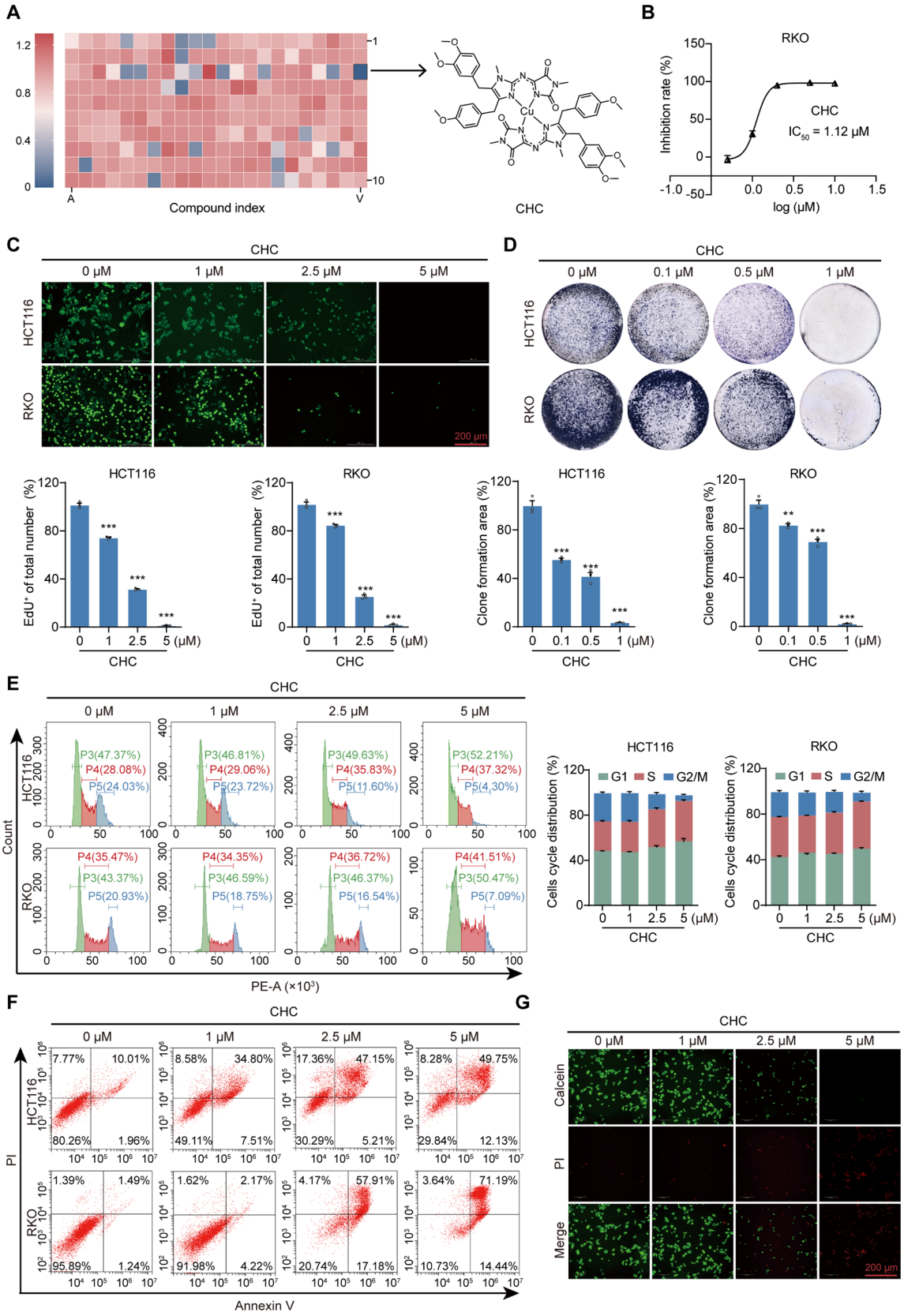

Figure 2. CHC shows significant cytotoxicity against colorectal cancer cells *in vitro*. (A) Screening of 220 molecules in the natural compound library. RKO cells were treated with drugs at 10 μM for 24 h, cell viability was determined via a CCK-8 assay, and the structure of CHC. (B) IC_{50} value of CHC in RKO cells (n = 3, error bars represent the SEM, mean ± SEM). (C) HCT116 and RKO cells were treated with CHC, and proliferation ability was detected via an EdU assay (scale bar: 200 μm) and quantified (n = 3, error bars represent the SEM, mean ± SEM, one-way ANOVA, compared with the control group). (D) HCT116 and RKO cells were treated with CHC, and colony formation ability was detected via crystal violet staining and quantified (n = 3, error bars represent the SEM, mean ± SEM, one-way ANOVA, compared with the control group). (E)

https://doi.org/10.1021/jacs.5c07917
J. Am. Chem. Soc. 2025, 147, 37089−37103

Figure 2. continued

HCT116 and RKO cells were treated with CHC, and cell cycle progression was detected via flow cytometry and quantified (n = 3, error bars represent the SEM, mean ± SEM, two-way ANOVA, compared with the control group). (F) HCT116 and RKO cells were treated with CHC, and cell death was detected via flow cytometry. (G) HCT116 cells were treated with CHC, and cell death was detected via calcein-AM/PI staining (scale bar: 200 μm). *p < 0.05, **p < 0.01, ***p < 0.001.

crystal X-ray diffraction on CHC and $Zn(NJ)_2$ for the first time to confirm the synthesized structures, which were also effectively validated by high-resolution mass spectrometry (Figure 1 and Supporting Information I).

CHC Exhibits Pronounced Cytotoxic Effects on Colorectal Cancer Cells *In Vitro*. We utilized the colorectal cancer cell line RKO as a model to screen a library of marine-derived natural compounds that could induce significant toxicity in RKO cells. The selected compounds were administered to the RKO cells at a concentration of 10 μM, and the cell viability was determined via the CCK-8 assay. As shown in Figure 2A, we identified a compound, CHC, that significantly inhibited the activity of RKO cells. We subsequently conducted further evaluations to assess the antitumor efficacy of CHC. CCK-8 assays demonstrated that CHC significantly inhibited the growth of both HCT116 and RKO colorectal cancer cells within the concentration range of 0−10 μM, with IC_{50} values of 0.79 μM and 1.12 μM, respectively (Figures 2B and S1A−C). To evaluate the inhibitory effect of CHC on the proliferation of HCT116 and RKO cells, an EdU assay was employed. The results indicated that exposure to CHC substantially inhibited cell proliferation (Figure 2C). Next, a colony formation assay revealed that treatment with CHC markedly reduced the colony-forming ability of both the HCT116 and RKO cell lines (Figure 2D). To determine whether the suppressive effect of CHC on cell proliferation was mediated through cell cycle inhibition, flow cytometry analysis was conducted. The results revealed that CHC treatment significantly induced G1 phase arrest in both HCT116 and RKO cells in a concentration-dependent manner (Figure 2E). Furthermore, the annexin V-FITC/PI double-staining assay confirmed that CHC treatment induced cell death in HCT116 and RKO cells in a concentration-dependent manner (Figures 2F and S1D). Additionally, the results of the calcein-AM/PI double-staining assay further demonstrated that CHC induced cell death in CRC cells in a dose-dependent manner (Figures 2G and S1E,F). In summary, CHC, which was selected from a marine-derived natural library, has a significant inhibitory effect on colorectal cancer cells.

CHC Induces Non-Apoptotic-Dependent Cell Death. Given the significant effects of CHC in inhibiting the viability of colorectal cancer cells, subsequent studies will delve into the specific pathways through which CHC induces tumor cell death. We applied a variety of inhibitors, including the ferroptosis inhibitors Lip-1 and DFO, the apoptosis inhibitor Z-VAD-FMK, and the necroptosis inhibitor Nec-1, to the RKO and HCT116 cell lines to investigate their effects on CHC-induced tumor cell death. The results showed that these inhibitors could not or only partially reversed CHC-induced cell death (Figure 3A−D). In subsequent experiments, we evaluated the cytotoxic effects of CHC on oxaliplatin-resistant HCT116 cells. As shown in Figure 3E, the IC_{50} values for oxaliplatin in HCT116 cells and oxaliplatin-resistant HCT116 cells were 21.65 and 107 μM, respectively. Similarly, the IC_{50} values for CHC in these two cell lines were 0.79 and 0.45 μM, respectively. These findings suggest that CHC possesses the capacity to counteract oxaliplatin resistance. To evaluate the inhibitory effect of CHC on the proliferation of HCT116 and RKO cells, flow cytometry analysis results revealed that CHC treatment significantly induced G2/M phase arrest in HCT116/OXA cells in a concentration-dependent manner (Figures 3F and S2A). Furthermore, a colony formation assay revealed that CHC significantly reduced the colony-forming ability of the HCT116/OXA cell line (Figures 3G and S2B). Consistent with these results, the results of EdU, annexin V-FITC/PI double-staining, and calcein-AM/PI double-staining assays also revealed that CHC significantly induced the death of HCT116/OXA cells (Figures 3H−J and S2C−E).

CHC Causes Cell Death in a Copper-Dependent Manner. CHC is a marine natural product formed by the complexation of two naamidine J monomer molecules with divalent copper ions. Studies have shown that naamidine J has low toxicity toward colorectal cancer cells.[22] To ascertain whether the cytotoxicity of CHC is associated with copper ions, we synthesized structural analogs of CHC with divalent nickel, cobalt, and zinc ions. These results indicated that these analogs had lower cytotoxicity than CHC did, suggesting that copper ions may play a crucial role in the cytotoxicity of CHC (Figure 4A). To further validate the role of copper ions in CHC, we cotreated RKO or HCT116 cells with copper gluconate and naamidine J. The results demonstrated that this combined treatment significantly inhibited the viability of RKO or HCT116 cells, similar to the effect of CHC, indicating that the presence of copper gluconate in the cell culture medium can facilitate the formation of CHC from naamidine J, which is cytotoxic (Figures 4B−D and S3A−E). To further establish the relationship between copper ions and cytotoxicity, CHC was coincubated with the copper ion chelator TTM in RKO cells. As shown in Figure 4E, the inhibitory effect of CHC on cell growth was negated, indicating that the cytotoxic effect of CHC is contingent upon copper ions. Moreover, similar results were observed in both RKO and HCT116/OXA cells (Figure S4A,C).

CHC Suppresses Colorectal Tumor Growth in Mice. Given the significant inhibitory effects of CHC on colorectal cancer cells *in vitro*, we further explored its antitumor activity *in vivo*. By subcutaneously inoculating the Luc-HCT116 cell line into BALB/c nude mice, we established control groups and treatment groups with varying doses of CHC (10, 20, and 40 mg/kg). We assessed the antitumor effects of CHC by comparing the tumor growth inhibition in Luc-HCT116 nude mice treated with CHC (0, 10, 20, and 40 mg/kg) over 12 consecutive days (Figure 5A). The results revealed that tumor growth was rapid in the control group, whereas in Luc-HCT116 tumor-bearing nude mice treated with CHC, tumor growth was effectively inhibited in a dose-dependent manner (Figure 5B). Consistent with the rate of tumor growth inhibition, CHC treatment significantly reduced tumor volume, with inhibition rates of 46.2%, 69.4%, and 78.2% at 10, 20, and 40 mg/kg, respectively (Figure 5C,F). Moreover, the average tumor weight in the CHC treatment groups was

https://doi.org/10.1021/jacs.5c07917
J. Am. Chem. Soc. 2025, 147, 37089−37103

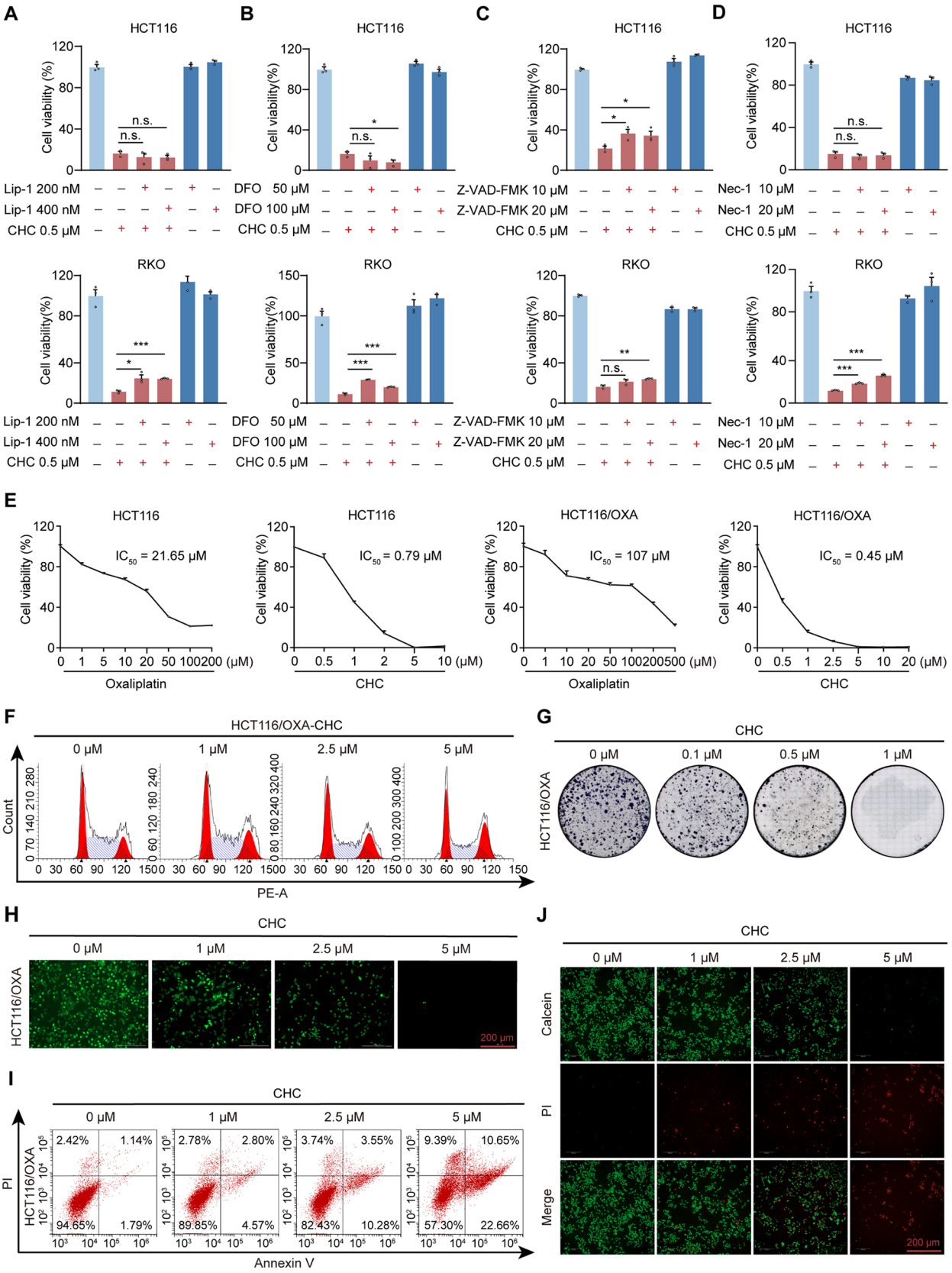

Figure 3. The cytotoxic effects of CHC are independent of the apoptotic pathway. (A–D) HCT116 and RKO cells were cotreated with CHC and Lip-1, DFO, Z-VAD-FMK, or Nec-1, and cell viability was determined via a CCK-8 assay (n = 3, error bars represent the SEM, mean ± SEM, t-test, compared with the CHC 0.5 μM group). (E) IC_{50} values of CHC and oxaliplatin in HCT116 and HCT116/OXA cells (n = 3, error bars represent the SEM, mean ± SEM). (F) HCT116/OXA cells were treated with CHC, and cell cycle progression was detected via flow cytometry. (G) HCT116/OXA cells were treated with CHC, and colony formation ability was detected via crystal violet staining. (H) HCT116/OXA cells were treated with CHC, and cell proliferation ability was detected via an EdU assay (scale bar: 200 μm). (I,J) HCT116/OXA cells were treated with

https://doi.org/10.1021/jacs.5c07917
J. Am. Chem. Soc. 2025, 147, 37089−37103

Figure 3. continued

CHC, and cell death was detected via flow cytometry and calcein-AM/PI staining (scale bar: 200 μm). n.s., not significant, *p < 0.05, **p < 0.01, ***p < 0.001.

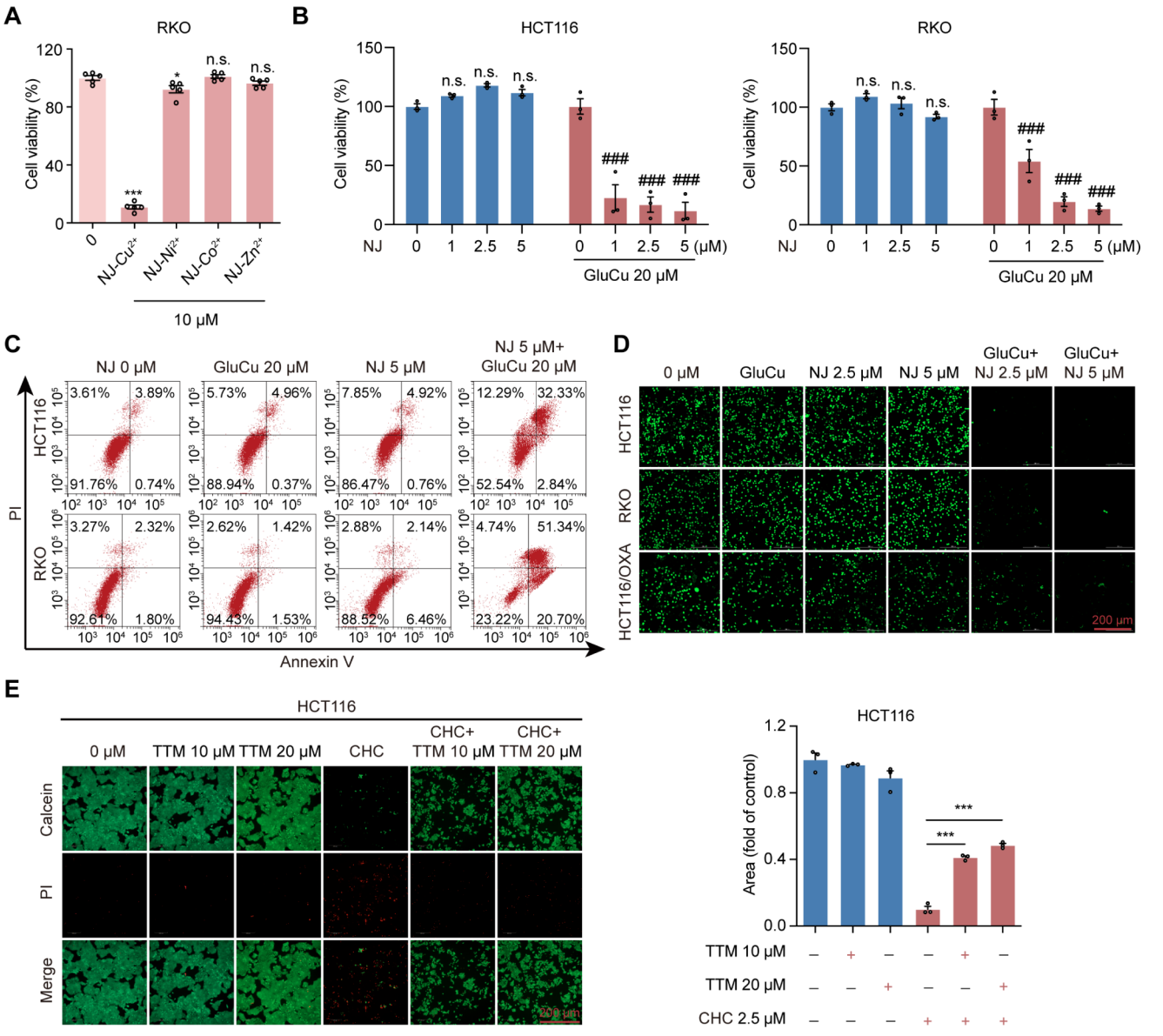

Figure 4. Copper ions act as a central effector in CHC-induced cell death. (A) RKO cells were treated with CHC, $Ni(NJ)_2$, $Co(NJ)_2$, or $Zn(NJ)_2$, and cell viability was determined via a CCK-8 assay (n = 5, error bars represent the SEM, mean ± SEM, one-way ANOVA, compared with the control group). (B,C) HCT116 and RKO cells were treated with naamidine J and GluCu (20 μM), and cell viability was determined via a CCK-8 assay (n = 3, error bars represent the SEM, mean ± SEM, two-way ANOVA, the blue bar chart compared with the NJ 0 μM group, the pink bar chart compared with the NJ 0 μM + GluCu 20 μM group) and flow cytometry. (D) HCT116, RKO, and HCT116/OXA cells were treated with naamidine J and GluCu (20 μM), and cell proliferation ability was detected via an EdU assay (scale bar: 200 μm). (E) HCT116 cells were treated with CHC (2.5 μM) and TTM, and the cells were stained with calcein-AM/PI (scale bar: 200 μm) and quantified (n = 3, error bars represent the SEM, mean ± SEM, t-test, compared with the CHC 2.5 μM group). n.s., not significant, *p < 0.05, ***p < 0.001, $^{###}p$ < 0.001.

significantly lower than that in the control group (Figure 5D). Additionally, we measured the tumor fluorescence intensity in each group at 0, 3, 6, and 12 days, and the results also indicated that CHC dose-dependently inhibited tumor growth (Figure 5G). Moreover, the immunohistochemical results revealed that the levels of Ki-67 (a proliferation marker) and LIAS (a Fe−S cluster protein) were significantly reduced in tumors, whereas HSP70 was increased after CHC treatment (Figures 5H and S5), indicating significant growth inhibition and cuproptosis of tumor cells in CHC-treated mice. Furthermore, CHC did not cause significant changes in mouse body weight at the dose of 40 mg/kg, suggesting that CHC did not lead to obvious toxic effects (Figure 5E).

CHC Induces Tumor Cuproptosis by Increasing ROS Level. To explore the molecular mechanisms underlying CHC-induced cell death, we performed transcriptome

https://doi.org/10.1021/jacs.5c07917
J. Am. Chem. Soc. 2025, 147, 37089−37103

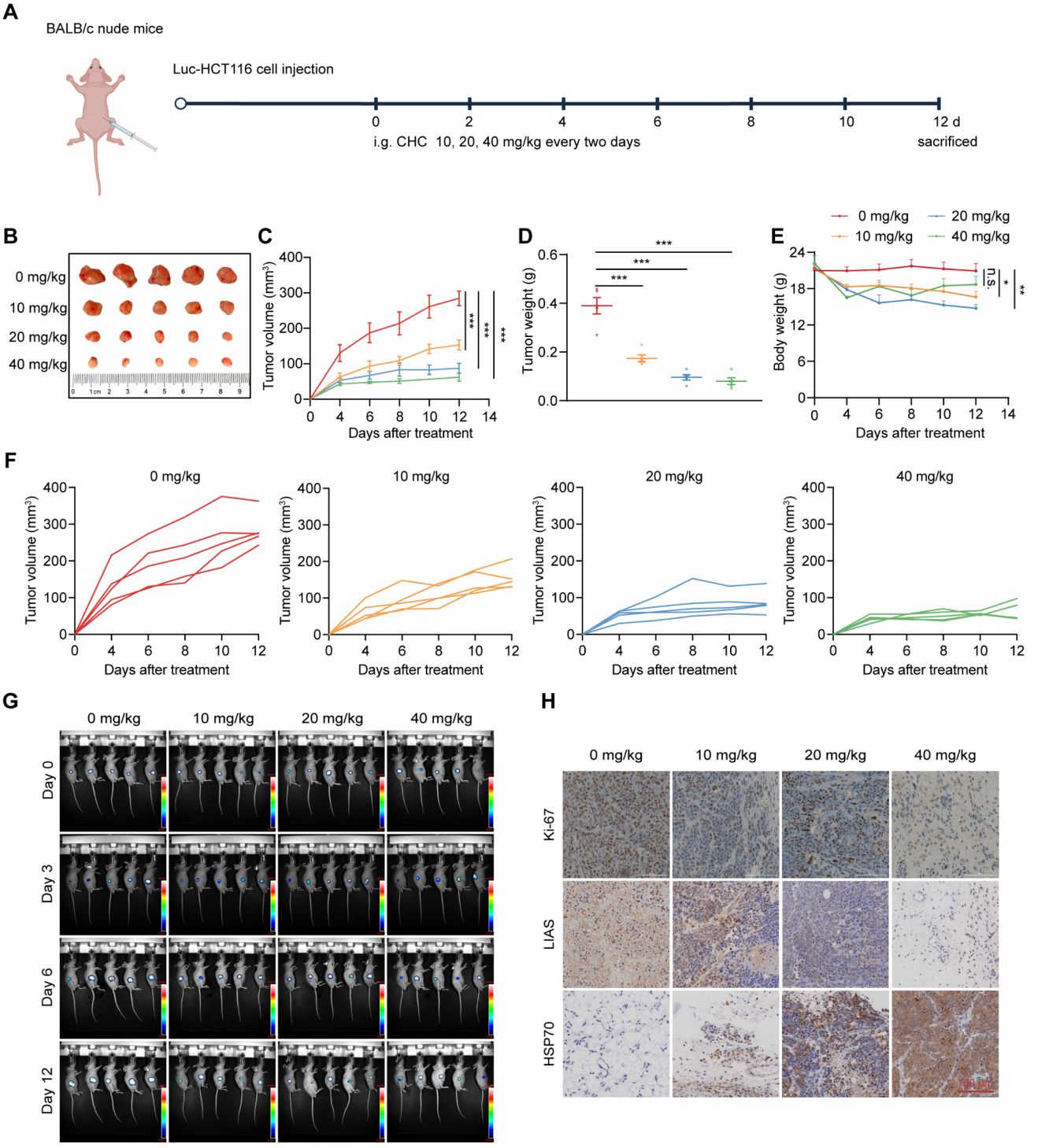

Figure 5. CHC treatment inhibited tumor growth *in vivo*. (A) Luc-HCT116 cells were injected into BALB/c nude mice, and 0, 10, 20, and 40 mg/kg CHC were administered via intragastric administration. (B) *Ex vivo* observation of the tumors from the treated mice. (C) BALB/c nude mice with Luc-HCT116 tumors were treated with CHC, and tumor growth was monitored (n = 5, error bars represent the SEM, mean ± SEM, one-way ANOVA, compared with the 0 mg/kg group). (D) Comparison of the weights of the tumors from the mice treated with CHC (n = 5, error bars represent the SEM, mean ± SEM, one-way ANOVA, compared with the 0 mg/kg group). (E) Body weight of the mice was measured every 2 days (n = 5, error bars represent the SEM, mean ± SEM, one-way ANOVA, compared with the 0 mg/kg group). (F) Tumor volume growth curves for single mice in 0 mg/kg, 10 mg/kg, 20 mg/kg, and 40 mg/kg groups. (G) Real-time tumor imaging of the mice during the experimental period. (H) Immunohistochemical staining results of Ki-67, LIAS, and HSP70 in BALB/c nude mice from different treatment groups (scale bar: 100 μm). n.s., not significant, *p < 0.05, **p < 0.01, ***p < 0.001.

sequencing analysis on RKO cells treated with CHC. In RKO cells, we identified 724 differentially expressed genes (FDR < 0.1, fold change ≥ 2). In the CHC-treated group, 678 genes were upregulated, and 46 genes were downregulated. Notably, several genes related to the heat shock response, such as HSPA6, were upregulated (Figure 6A). KEGG pathway

https://doi.org/10.1021/jacs.5c07917
J. Am. Chem. Soc. 2025, 147, 37089−37103

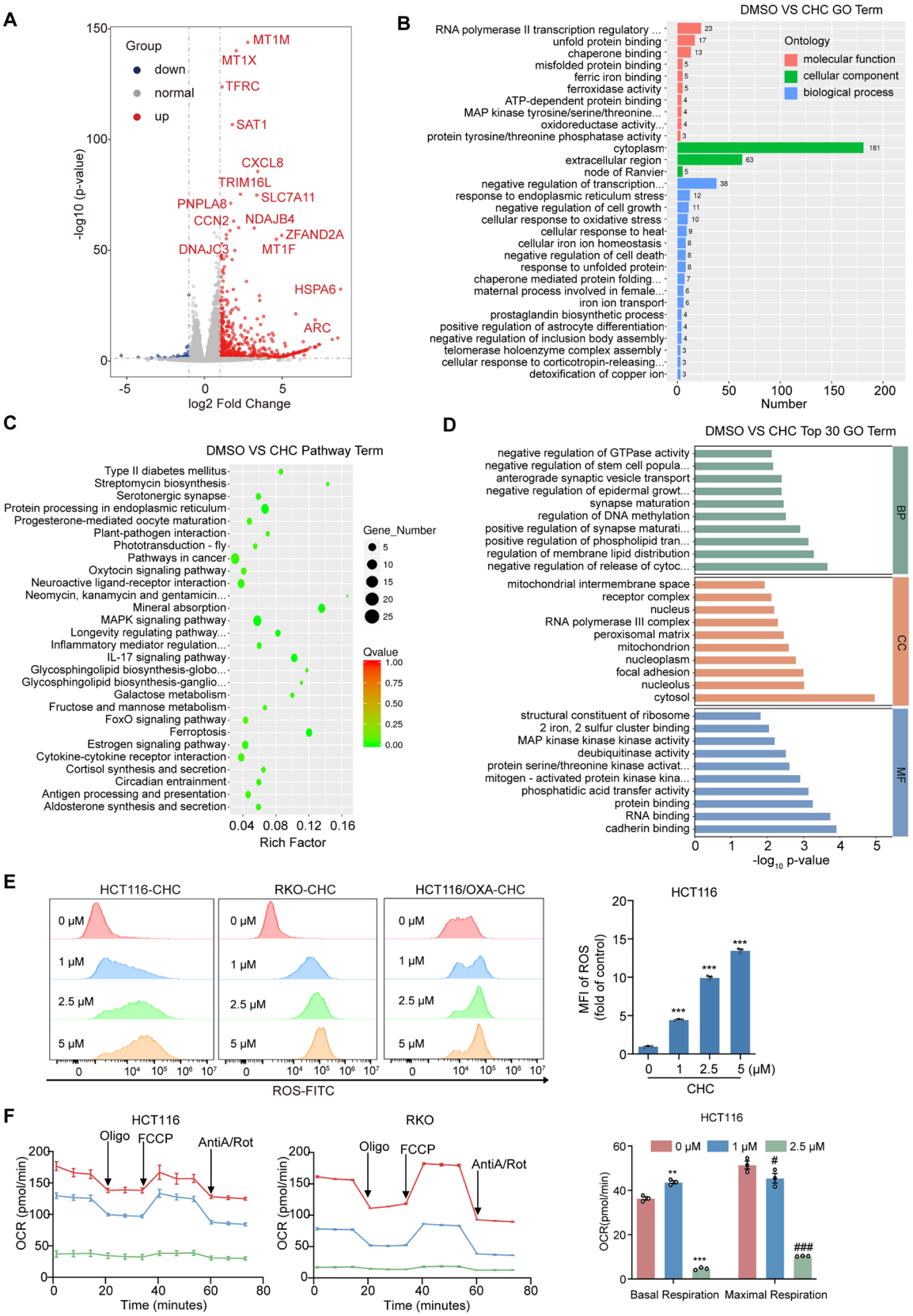

Figure 6. CHC upregulates ROS level, leading to cell death in colorectal cancer cells. (A) The volcano plot illustrates the changes in mRNA levels after CHC treatment in RKO cells. (B) Gene Ontology analysis of differentially expressed mRNAs in RKO cells after CHC treatment. (C) KEGG analysis of differentially expressed mRNAs in CHC-treated RKO cells. (D) Gene Ontology analysis of differentially expressed proteins in RKO cells after CHC treatment. (E) HCT116, RKO, and HCT116/OXA cells were treated with CHC, and the level of ROS in the cells was detected via flow cytometry and quantified (n = 3, error bars represent the SEM, mean ± SEM, one-way ANOVA, compared with the 0 μM group). (F) HCT116 and RKO cells were treated with CHC, the oxygen consumption rate was detected with an Agilent Seahorse XFe96, and quantified (n = 3, error

https://doi.org/10.1021/jacs.5c07917
J. Am. Chem. Soc. 2025, 147, 37089−37103

Figure 6. continued

bars represent the SEM, mean ± SEM, two-way ANOVA, * compared with the basal respiration 0 μM group, # compared with the maximal respiration 0 μM group). $^{**}p < 0.01$, $^{***}p < 0.001$, $^{\#}p < 0.05$, $^{\#\#\#}p < 0.001$.

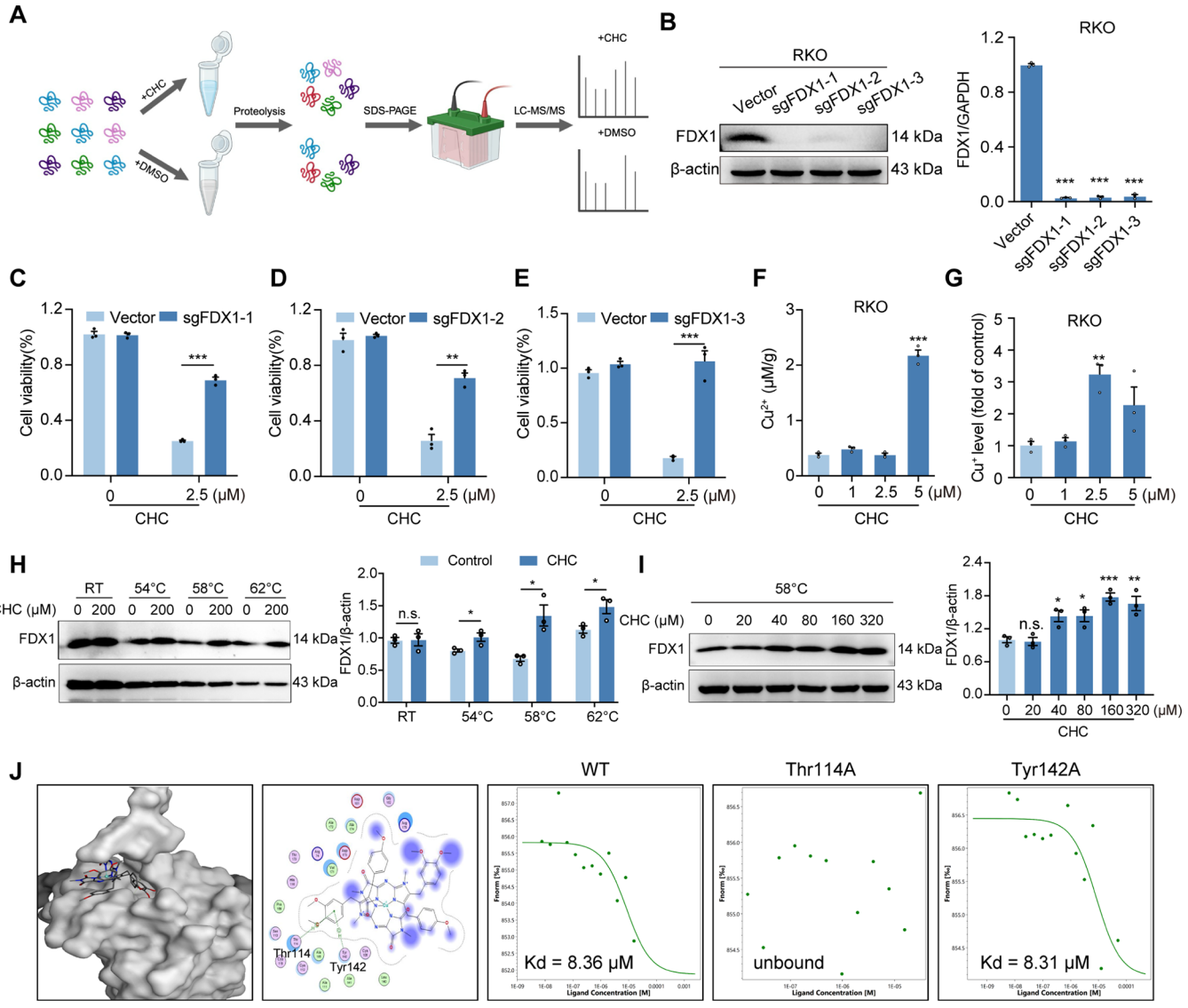

Figure 7. CHC exerts antitumor effects by directly targeting FDX1. (A) Flowchart of DARTS. (B) FDX1 levels were detected after knockout in RKO cells, and FDX1 intensity was quantified (n = 3, error bars represent the SEM, mean ± SEM, one-way ANOVA, compared with the Vector group). (C−E) RKO cells with *FDX1* knockout were treated with CHC, and cell viability was determined via a CCK-8 assay (n = 3, error bars represent the SEM, mean ± SEM, t-test, compared with the Vector + CHC 2.5 μM group). (F) RKO cells were treated with CHC, and the level of Cu^{2+} in cells was detected (n = 3, error bars represent the SEM, mean ± SEM, one-way ANOVA, compared with the 0 μM group). (G) RKO cells were treated with CHC, and the level of Cu^{+} in cells was detected (n = 3, error bars represent the SEM, mean ± SEM, one-way ANOVA, compared with the 0 μM group). (H) CETSA was used to determine the thermal stabilization of the FDX1 interaction with CHC at a series of temperatures from 54 to 62 °C, and FDX1 intensity was quantified (n = 3, error bars represent the SEM, mean ± SEM, t-test, compared with the control group). (I) Effects of different concentrations of CHC on FDX1 protein stability at 58 °C, and FDX1 intensity was quantified (n = 3, error bars represent the SEM, mean ± SEM, one-way ANOVA, compared with the 0 μM group). (J) Molecular docking of CHC to FDX1 (3n9y) and the cellular MST assay of GFP-tagged FDX1 upon overexpression of wild-type FDX1 and the disruptive mutants. n.s., not significant, $^{*}p < 0.05$, $^{**}p < 0.01$, $^{***}p < 0.001$.

analysis revealed the enrichment of genes associated with protein processing in the endoplasmic reticulum (Figure 6C). Additionally, the GO pathway enrichment analysis revealed the enrichment of genes related to misfolded protein binding, cellular response to oxidative stress, and cellular response to heat (Figure 6B). These results suggest that CHC may induce proteotoxic stress and trigger heat shock responses, leading to cell death. Consistent with this expectation, proteomic analysis also revealed that reactive oxygen species were significantly increased following CHC treatment (Figure S6A). As shown in Figure 6D, mitochondrion and iron−sulfur cluster binding were enriched. In summary, we preliminarily speculate that CHC may induce cell death by increasing the level of ROS. Further experiments conducted in RKO, HCT116, and

https://doi.org/10.1021/jacs.5c07917
J. Am. Chem. Soc. 2025, 147, 37089−37103

HCT116/OXA cells demonstrated the impact of CHC on ROS level, showing that CHC can increase ROS levels in a dose-dependent manner (Figures 6E and S6B). Additionally, CHC dose-dependently disrupted mitochondrial function in RKO and HCT116 cells and significantly inhibited basal cellular respiration and maximum cellular respiration capacity (Figures 6F and S6C).

CHC Exerts Antitumor Effects by Directly Targeting FDX1. To explore the potential targets of CHC in inducing tumor cell death, we utilized drug affinity responsive target stability (DARTS) to identify proteins that directly interact with CHC. The DARTS process is illustrated in Figure 7A. Using the DARTS technique combined with proteomic analysis, our study initially identified 129 potential small-molecule binding proteins from cell lysates, which met the stringent criteria of ≥2 characteristic peptides and an intensity ratio of ≥1.5. Through integrated bioinformatic filtering, affinity-based ranking, and literature validation of known oncology-related targets, nine high-confidence candidates were prioritized for experimental verification: oxidative stress regulators (SOD1, CCS, FDX1), cell cycle modulators (SKP2, PLK1), mitochondrial functional components (MTCO2, LRPPRC), and transcriptional regulators (ZMIZ1, PODXL2). We subsequently utilized siRNA interference technology to silence these genes and assessed the impact of CHC on RKO cell death (Figures S7A−E and S8A−C). Ultimately, we identified ferredoxin 1 (FDX1) as a potential target gene for CHC. We subsequently knocked out *FDX1* and found that the knockout of *FDX1* reversed the toxic effect of CHC on RKO cells (Figure 7B−E). FDX1 is a core molecule involved in copper death and is capable of reducing Cu^{2+} to more toxic Cu^{+}. When we measured the intracellular Cu^{+} concentration, the results revealed that CHC increased the Cu^{+} concentration in RKO cells, indicating that CHC induces tumor cell death by targeting FDX1 and subsequently elevating intracellular Cu^{+} concentrations (Figure 7F,G). To determine whether CHC directly binds to the FDX1 protein, we employed a cellular thermal shift assay (CETSA), which is based on the biophysical principle that potential target proteins exhibit thermal stability when they are bound to a ligand. To avoid protein metabolism cascades that might be induced by prolonged incubation with lysis buffer and drugs, we incubated the drug with lysis buffer for 1 min to detect direct interactions. As shown in Figure 7H, CHC significantly increased the accumulation of FDX1, suggesting that CHC directly interacts with FDX1. Consistent with the CETSA results, FDX1 also accumulated with increasing concentrations of CHC when under the condition of 58 °C (Figure 7I). We subsequently performed microscale thermophoresis (MST) to analyze the direct binding between CHC and GFP-tagged FDX1 proteins. As anticipated, CHC bound to FDX1, with a K_d value of 8.36 μM (Figure 7J). To identify the critical amino acid residues in FDX1 involved in CHC binding, molecular docking simulations were performed to model the interaction mode between CHC and FDX1. The docking results revealed that CHC formed hydrogen bonds and hydrophobic interactions with residues Thr114 and Tyr142 of FDX1. To validate these predicted binding sites, MST analysis was conducted to evaluate the binding affinity of FDX1-GFP mutants with CHC. The MST results showed that mutation of Tyr142 to alanine resulted in a dissociation constant (K_d = 8.31 μM) comparable to that of the wild-type protein (K_d = 8.36 μM), indicating the minimal contribution of this residue to binding affinity. In contrast, the mutation of Thr114 to alanine completely abolished CHC binding to FDX1, confirming Thr114 as an essential binding site. Collectively, these findings demonstrate that CHC targets the Thr114 residue of FDX1 to increase the Cu^{+} concentration in tumor cells, thereby inducing tumor cell death.

DISCUSSION

Copper plays a dual role in organisms and is an essential cofactor for numerous enzymes, yet even moderate intracellular concentrations can become toxic, leading to cell death. Genetic variations in copper homeostasis can cause severe, life-threatening diseases. Copper ionophores and copper chelators are both considered anticancer agents. In this study, we identified CHC from a library of marine-derived compounds that have significant anticolorectal cancer effects. Mechanistic studies indicate that the mechanism of action of CHC differs from those of apoptosis and necrosis, as it targets FDX1 and upregulates the expression of Cu^{+} in tumor cells, thereby inducing tumor cell death. Functionally, CHC significantly inhibits the growth of colorectal cancer both *in vitro* and *in vivo*, providing a new therapeutic approach for cancer treatment.

Copper homeostasis in tumors is a critical factor, with alterations potentially leading to the development of copper-coordinated compounds for anticancer therapy. Currently, there are two main strategies targeting copper homeostasis: one is the use of copper chelators to reduce the bioavailability of copper, and the other is the use of copper ionophores to increase intracellular copper levels by delivering copper into cells.[24] Various copper chelators, such as tetrathiomolybdate (TTM), trientine, and d-penicillamine, have been developed and evaluated for their antitumor effects in animal models and clinical trials.[25,26] Concurrently, several copper ionophores, including elesclomol, bis(thiosemicarbazone) analogs [CuII-(atsm) and CuII(gtsm)], and disulfiram (DSF), have been shown to increase intracellular copper levels and exhibit anticancer activity.[27,28] The cytotoxic effects of these copper ionophores on cancer cells may be partly attributed to their ability to increase the production of reactive oxygen species (ROS) and/or inhibit the proteasome.[29,30] Specifically, combination treatment with DSF and copper has been shown to decrease the expression of the tumor suppressor gene PTEN in human breast cancer cells and activate the AKT signaling pathway, providing a theoretical basis for future therapeutic strategies that combine copper ionophores with PI3K-AKT inhibitors.[31,32] Elesclomol, a novel copper ionophore, has been demonstrated to import copper into mitochondria, thereby increasing oxidative stress and inducing cell death.[33−35] In our study, CHC significantly upregulated the expression of ROS in tumor cells and increased the concentration of copper ions within the tumor cells. However, when the copper ions in the CHC were replaced with cobalt or zinc ions, the cytotoxicity significantly decreased. Notably, when TTM and CHC were added together, TTM was able to completely reverse the cell death induced by CHC. Additionally, when naamidine J and copper gluconate were simultaneously added to the cell culture medium, the cytotoxicity was significantly enhanced. Therefore, CHC may achieve its cytotoxic effects on tumor cells by increasing the concentration of copper ions in tumor cells.

Ferredoxin 1 (FDX1) is a small iron−sulfur protein that transfers electrons from NADPH to cytochrome P450 in the

https://doi.org/10.1021/jacs.5c07917
J. Am. Chem. Soc. 2025, 147, 37089−37103

mitochondria through the action of ferredoxin reductase (FDXR). It is involved in the metabolism of steroids, cholesterol, and bile acids.[36,37] Recent studies have revealed that FDX1 is closely associated with copper-dependent cell death, known as cuproptosis.[11,38−40] FDX1 can upregulate protein lipoylation, reducing Cu^{2+} to the more toxic Cu^{+}, and the loss of FDX1 confers resistance to copper-induced cell death.[41−43] In this study, we used the DARTS/MS method to screen for potential targets of CHC, and the results indicated that FDX1 is a primary target of CHC. Further experiments demonstrated that the knockdown of FDX1 reversed the toxic effects of CHC on RKO colorectal cancer cells, suggesting that FDX1 plays a critical role in CHC-induced cell death. As a central molecule in copper-induced cell death, FDX1 facilitates the reduction of Cu^{2+} to the more toxic Cu^{+}. Subsequent MST experiments confirmed that CHC directly interacts with FDX1, further suggesting that CHC may induce tumor cell death by targeting FDX1 to increase Cu^{+} levels. Additionally, our research revealed that CHC effectively overcame oxaliplatin resistance in HCT116 cells, and the cytotoxic effect of CHC on normal HCT116 cells was comparable to that on resistant cells. Animal studies further demonstrated that CHC can inhibit the growth of colorectal cancer in a dose-dependent manner, highlighting its substantial potential for clinical therapy.

CONCLUSIONS

Our research demonstrated that CHC targets FDX1 to increase the intracellular Cu^{+} concentration, thereby inducing tumor cell death. Moreover, CHC shows significant efficacy in overcoming the resistance of colon cancer cells to oxaliplatin. Additionally, CHC exhibited strong antitumor activity in a mouse colon cancer model, offering new hope for the treatment of resistant tumors. These findings suggest that CHC has a strong potential for clinical application and may be a novel therapeutic option for colorectal cancer treatment.

EXPERIMENTAL SECTION

Antibodies and Reagents. All of the antibodies and reagents used are listed in Table S1.

Cell Culture. RKO cells were grown in MEM (Meilunbio, Dalian, China) supplemented with 10% fetal bovine serum (Biological Industries, Cromwell, CT, USA) and 1% penicillin−streptomycin (Meilunbio, Dalian, China), and HCT116 cells were grown in McCoy's 5A medium (Meilunbio, Dalian, China) supplemented with 10% fetal bovine serum and 1% penicillin−streptomycin.

Immunoblotting. According to the protein quantification results, the protein samples were loaded to be separated into the wells of a 12% gel sequentially and perform electrophoresis. Subsequently, electrotransfer to a PVDF membrane, block the membrane with 5% nonfat milk powder at room temperature for 1 h, and wash the bands with 1× TBST. Incubate the membrane with the primary antibody against the target protein at 4 °C overnight. The next day, recover the primary antibody, and wash the bands with 1× TBST. Then incubate the membrane with the corresponding secondary antibody at room temperature for 1 h, recover the secondary antibody, and wash the bands again with 1× TBST. Finally, observe the bands using a gel imaging system (Bio-Rad, USA).

Cell Viability Assay. RKO and HCT116 cells were seeded into 96-well plates and then incubated with compounds at different concentrations. Through treatment at different time points, the effects of the compounds on cell viability were detected via a CCK-8 (Meilunbio, Dalian, China) according to the manufacturer's instructions.

EdU Staining. RKO and HCT116 cells were seeded into 12-well plates and then incubated with compounds at different concentrations. After incubation for 24 h, the effects of the compounds on cell proliferation were detected via an EdU Cell Proliferation Kit (Beyotime, Shanghai, China) according to the manufacturer's instructions.

Cell Colony Formation Assay. RKO and HCT116 cells were seeded in 12-well plates and then incubated with compounds at different concentrations. After incubation for several days, the culture was terminated, fixed with 4% paraformaldehyde, stained with crystal violet, and imaged with Cytation 5 (BioTek, USA).

Cell Cycle Analysis. RKO and HCT116 cells were seeded in six-well plates and then incubated with compounds at different concentrations. After incubation for hours, following the manufacturer's instructions for the Cell Cycle and Apoptosis Analysis Kit (Beyotime, Shanghai, China), the impact of the compounds on the cell cycle was assessed using a flow cytometer (Beckman Coulter CytoFLEX, USA).

Annexin V-FITC/PI Staining. RKO and HCT116 cells were seeded in 6-well plates, then incubated with compounds at different concentrations. After incubation for 24 h, according to the instructions of the Annexin V-FITC apoptosis assay kit (Beyotime, Shanghai, China), the effects of the drugs on cell cytotoxicity were detected via flow cytometry.

Calcein-AM/PI Staining. RKO and HCT116 cells were seeded in 96-well plates and then incubated with compounds at different concentrations. After incubation for 24 h, according to the instructions of the Calcein/PI Cell Viability/Cytotoxicity Assay Kit (Beyotime, Shanghai, China), the effects of the drugs on cell cytotoxicity were imaged with Cytation 5.

ROS Level Analysis. According to the ROS Assay Kit (Beyotime, Shanghai, China), the probe was added into the collected RKO and HCT116 cells, then incubated with different concentrations of CHC for several hours, and the level of ROS was detected using a flow cytometer.

Oxygen Consumption Rate Analysis. RKO and HCT116 cells were seeded in 96-well plates, then incubated with compounds at different concentrations. After incubation for 12 h, the cell culture medium was replaced with Seahorse XF detection solution, and oligomycin, FCCP, or AntiA/Rot was added. The oxygen consumption rate was detected with an Agilent Seahorse XFe96.

Drug Affinity-Responsive Target Stability. The RKO cell lysates were split into two equal groups, one treated with CHC (200 μM) and the other with DMSO, both incubated at room temperature for 1 h. Next, a suitable ratio of protease was added to the mixtures, which were then digested for 30 min. After digestion, 5× loading buffer was incorporated, and the samples were boiled at 95 °C for 5 min. Subsequently, the samples were separated via SDS-PAGE, stained using Coomassie brilliant blue dye, subjected to enzymolysis, and ultimately analyzed by LC-MS.

Quantitative Real-Time PCR. RKO cells were used for total RNA extraction with RNAiso Plus (Takara, Dalian, China). Following the manufacturer's instructions, 1 μg of the extracted RNA was converted to cDNA via reverse transcription using the PrimeScript RT Reagent Kit (Takara, Dalian, China). Subsequently, qRT-PCR was performed on a LightCycler 96 instrument (Roche, Basel, Switzerland). Ultimately, the results were normalized against the expression levels of the β-actin reference gene. The primer sequences utilized are listed in Table S2.

Cell Transfections for Gene Silencing. The siRNAs used in this study were obtained from GenePharma (Shanghai, China), and their specific sequences are listed in Table S3. A negative control (NC) was included as a reference. RKO cells were seeded into 6-well plates and allowed to culture for 24 h. Following this, siRNA transfection was performed using Lipofectamine 2000 (Invitrogen, Carlsbad, CA), and the cells were incubated for an additional 24 h.

CRISPR/Cas9 Gene Deletion. The LentiCRISPRv2 vector was used as a backbone to insert gRNAs targeting FDX1. BsmBI restriction enzyme digestion of the backbone vector was followed by T4 ligation. RKO cells were transfected with pAS2, pMD2.G, and

https://doi.org/10.1021/jacs.5c07917
J. Am. Chem. Soc. 2025, 147, 37089−37103

PlentiCRISPRv2 for control, and recombinant plasmids containing sgRNAs targeting FDX1 were subsequently placed under 2 μg/mL puromycin, and single clones were selected, grown, and validated. The sequences are shown in Table S3.

Cu^{2+} Level Assay. RKO cells were seeded in 10 cm plates containing different concentrations of drugs. The level of Cu^{2+} in the cells was detected via Cytation 5 following the operational guidelines of the Cell Copper (Cu^{2+}) Colorimetric Assay Kit (Elabscience, Wuhan, China).

Cu^{+} Level Assay. RKO cells were seeded in 10 cm plates containing different concentrations of the drugs. The level of Cu^{+} in the cells was detected via Cytation 5 following the operational guidelines of the Cellular Cuprous Fluorometric Assay Kit (Elabscience, Wuhan, China).

Cellular Thermal Shift Assay. The RKO cell lysates were split into two equal groups, one treated with CHC (200 μM) and the other with DMSO at room temperature for 1 min. The mixtures were divided, heated at different temperatures for 3 min, centrifuged, and 5× loading buffer was incorporated into the supernatant, boiled at 95 °C for 5 min, and stored at −20 °C.

Molecular Docking of CHC to FDX1. Obtain the molecular structure of compound CHC from the PubChem database (https://pubchem.ncbi.nlm.nih.gov/), import it into the MOE (Molecular Operating Environment) software, and run the Protonate 3D and Energy Minimize modules, respectively, to perform protonation and energy minimization operations. Retrieve the protein crystal structure of FDX1 (PDB ID: 3n9y) from the RCSB PDB database (https://www.rcsb.org/), import it into MOE, and run the QuickPrep module. This module will remove water molecules outside the 4.5 Å range of the protein and perform operations such as completing the missing side chains of the protein, adding hydrogen for protonation, and energy optimization. Use the DOCK module in MOE for molecular docking calculations, set the original ligand-binding pocket as the binding site for this molecular docking, set the refinement method to Induced Fit, and keep other parameters as default. After the molecular docking calculation is completed, we select the docking results with the top scores to analyze the potential binding mode between compound CHC and FDX1.

Microscale Thermophoresis. To confirm the binding capacity of CHC to wild-type or mutant FDX1, three plasmids encoding the GFP-tagged target protein were expressed in 293T cells. After 48 h, cell lysates were prepared and subsequently analyzed using the Monolith™ NT.115 MST system (NanoTemper, Germany).

Mouse Xenograft Model. For the Luc-HCT116 xenograft model, 1×10^6 Luc-HCT116 cells were injected into BALB/c nude mice subcutaneously. Once the average tumor volume reached roughly 50 mm^3, the mice were randomly assigned to four groups, and each group received intragastric administration at doses of 0, 10, 20, and 40 mg/kg CHC, respectively. Additionally, the tumors and body weights were measured and imaged *in vivo* every 2 days for 12 days.

Statistical Analysis. Statistical analysis was performed with a *t*-test when two different groups were compared and one-way or two-way ANOVA for comparisons among multiple groups. All the statistical analysis results are presented as the mean ± SEM using GraphPad Prism 9.

■ ASSOCIATED CONTENT

Data Availability Statement

The data that support the findings of this study are available from the corresponding author upon reasonable request.

Supporting Information

The Supporting Information is available free of charge at https://pubs.acs.org/doi/10.1021/jacs.5c07917.

The chemical experimental section (PDF)

The biological experimental section (PDF)

Accession Codes

Deposition Numbers 2434914 and 2445983 contain the supplementary crystallographic data for this paper. These data can be obtained free of charge via the joint Cambridge Crystallographic Data Centre (CCDC) and Fachinformationszentrum Karlsruhe Access Structures service.

■ AUTHOR INFORMATION

Corresponding Authors

Weidong Zhang − *Department of Phytochemistry, School of Pharmacy, Second Military Medical University, Shanghai 200433, China; Institute of Medicinal Plant Development, Chinese Academy of Medical Sciences and Peking Union Medical College, Beijing 100193, China*; Email: wdzhangy@hotmail.com

Sanhong Liu − *State Key Laboratory of Discovery and Utilization of Functional Components in Traditional Chinese Medicine, Shanghai Frontiers Science Center of TCM Chemical Biology, Institute of Interdisciplinary Integrative Medicine Research, Shanghai University of Traditional Chinese Medicine, Shanghai 201203, China*; orcid.org/0000-0002-8695-0343; Email: liush@shutcm.edu.cn

Xu-Wen Li − *State Key Laboratory of Chemical Biology, Shanghai Institute of Materia Medica, Chinese Academy of Sciences, Shanghai 201203, China; Shandong Laboratory of Yantai Drug Discovery, Bohai rim Advanced Research Institute for Drug Discovery, Yantai 264117, China*; orcid.org/0000-0001-7919-9726; Email: xwli@simm.ac.cn

Yue-Wei Guo − *Shandong Laboratory of Yantai Drug Discovery, Bohai rim Advanced Research Institute for Drug Discovery, Yantai 264117, China*; orcid.org/0000-0003-0413-2070; Email: ywguo@simm.ac.cn

Authors

Xiaoyu Tao − *State Key Laboratory of Discovery and Utilization of Functional Components in Traditional Chinese Medicine, Shanghai Frontiers Science Center of TCM Chemical Biology, Institute of Interdisciplinary Integrative Medicine Research, Shanghai University of Traditional Chinese Medicine, Shanghai 201203, China; State Key Laboratory of Chemical Biology, Shanghai Institute of Materia Medica, Chinese Academy of Sciences, Shanghai 201203, China; Shandong Laboratory of Yantai Drug Discovery, Bohai rim Advanced Research Institute for Drug Discovery, Yantai 264117, China*

Hongru Wang − *State Key Laboratory of Discovery and Utilization of Functional Components in Traditional Chinese Medicine, Shanghai Frontiers Science Center of TCM Chemical Biology, Institute of Interdisciplinary Integrative Medicine Research, Shanghai University of Traditional Chinese Medicine, Shanghai 201203, China*

Qun Wang − *State Key Laboratory of Discovery and Utilization of Functional Components in Traditional Chinese Medicine, Shanghai Frontiers Science Center of TCM Chemical Biology, Institute of Interdisciplinary Integrative Medicine Research, Shanghai University of Traditional Chinese Medicine, Shanghai 201203, China*

Chengji Wang − *Shanghai Laboratory Animal Research Center, Shanghai 201203, China*

Chang-Wei Shao − *Shandong Laboratory of Yantai Drug Discovery, Bohai rim Advanced Research Institute for Drug Discovery, Yantai 264117, China*

Yang Jin − *State Key Laboratory of Chemical Biology, Shanghai Institute of Materia Medica, Chinese Academy of Sciences, Shanghai 201203, China; Shandong Laboratory of Yantai Drug Discovery, Bohai rim Advanced Research Institute for Drug Discovery, Yantai 264117, China*
Dianping Yu − *State Key Laboratory of Discovery and Utilization of Functional Components in Traditional Chinese Medicine, Shanghai Frontiers Science Center of TCM Chemical Biology, Institute of Interdisciplinary Integrative Medicine Research, Shanghai University of Traditional Chinese Medicine, Shanghai 201203, China*
Hongmei Hu − *State Key Laboratory of Discovery and Utilization of Functional Components in Traditional Chinese Medicine, Shanghai Frontiers Science Center of TCM Chemical Biology, Institute of Interdisciplinary Integrative Medicine Research, Shanghai University of Traditional Chinese Medicine, Shanghai 201203, China*
Qing Zhang − *State Key Laboratory of Discovery and Utilization of Functional Components in Traditional Chinese Medicine, Shanghai Frontiers Science Center of TCM Chemical Biology, Institute of Interdisciplinary Integrative Medicine Research, Shanghai University of Traditional Chinese Medicine, Shanghai 201203, China*
Mengting Xu − *State Key Laboratory of Discovery and Utilization of Functional Components in Traditional Chinese Medicine, Shanghai Frontiers Science Center of TCM Chemical Biology, Institute of Interdisciplinary Integrative Medicine Research, Shanghai University of Traditional Chinese Medicine, Shanghai 201203, China*
Xiangxin Geng − *State Key Laboratory of Discovery and Utilization of Functional Components in Traditional Chinese Medicine, Shanghai Frontiers Science Center of TCM Chemical Biology, Institute of Interdisciplinary Integrative Medicine Research, Shanghai University of Traditional Chinese Medicine, Shanghai 201203, China*
Hanchi Xu − *State Key Laboratory of Discovery and Utilization of Functional Components in Traditional Chinese Medicine, Shanghai Frontiers Science Center of TCM Chemical Biology, Institute of Interdisciplinary Integrative Medicine Research, Shanghai University of Traditional Chinese Medicine, Shanghai 201203, China*
Linyang Li − *State Key Laboratory of Discovery and Utilization of Functional Components in Traditional Chinese Medicine, Shanghai Frontiers Science Center of TCM Chemical Biology, Institute of Interdisciplinary Integrative Medicine Research, Shanghai University of Traditional Chinese Medicine, Shanghai 201203, China*
Ruling Shen − *Shanghai Laboratory Animal Research Center, Shanghai 201203, China*

Complete contact information is available at: https://pubs.acs.org/10.1021/jacs.5c07917

Author Contributions

[▽]X.T., H.W., Q.W., and C.W. contributed equally to this work.

Notes

The authors declare no competing financial interest.

■ ACKNOWLEDGMENTS

This research was funded by the National Natural Science Foundation of China (82141203, 82374086, 82104459, 82022069), the National Key Research and Development Program of China (No. 2022YFC3502000, 2021YFF0502400), the Shanghai Municipal Science and Technology Major Project (ZD2021CY001), the Innovation Team and Talents Cultivation Program of the National Administration of Traditional Chinese Medicine (ZYYCXTDD-202004), the Strategic Priority Research Program of the Chinese Academy of Sciences (XDB1060000), the Key R&D Program of Shandong Province (2024CXPT028), the Taishan Scholars Program (tsqn2023-12302), the Key Marine Service Industry Program of Shandong Province, the Science and Technology Commission of Shanghai Municipality (20YF1458700), the Organizational Key Research and Development Program of Shanghai University of Traditional Chinese Medicine (2023YZZ02), the CAMS Innovation Fund for Medical Sciences (CIFMS) (2023-I2M-3-009), and the Key Project at Central Government Level: The Ability Establishment of Sustainable Use for Valuable Chinese Medicine Resources (2060302-2305-02). We thank the staff members of the Large-scale Protein Preparation System at the National Facility for Protein Science in Shanghai (NFPS), Shanghai Advanced Research Institute, Chinese Academy of Sciences, China, for providing technical support and assistance in data collection and analysis.

■ REFERENCES

(1) Bray, F.; Laversanne, M.; Sung, H.; Ferlay, J.; Siegel, R. L.; Soerjomataram, I.; Jemal, A. Global cancer statistics 2022: GLOBOCAN estimates of incidence and mortality worldwide for 36 cancers in 185 countries. *CA Cancer J. Clin.* **2024**, *74* (3), 229−263.
(2) Xi, Y.; Xu, P. Global colorectal cancer burden in 2020 and projections to 2040. *Transl. Oncol.* **2021**, *14*, 101174.
(3) Nussinov, R.; Tsai, C. J.; Jang, H. Anticancer drug resistance: An update and perspective. *Drug Resist. Updates* **2021**, *59*, 100796.
(4) Van der Jeught, K.; Xu, H.-C.; Li, Y.-J.; Lu, X.-B.; Ji, G. Drug resistance and new therapies in colorectal cancer. *World J. Gastroenterol.* **2018**, *24* (34), 3834−3848.
(5) Chen, L.; Min, J.; Wang, F. Copper homeostasis and cuproptosis in health and disease. *Signal Transduct. Target. Ther.* **2022**, *7* (1), 378.
(6) Ge, E. J.; Bush, A. I.; Casini, A.; Cobine, P. A.; Cross, J. R.; DeNicola, G. M.; Dou, Q. P.; Franz, K. J.; Gohil, V. M.; Gupta, S.; Kaler, S. G.; Lutsenko, S.; Mittal, V.; Petris, M. J.; Polishchuk, R.; Ralle, M.; Schilsky, M. L.; Tonks, N. K.; Vahdat, L. T.; Van Aelst, L.; Xi, D.; Yuan, P.; Brady, D. C.; Chang, C. J. Connecting copper and cancer: From transition metal signalling to metalloplasia. *Nat. Rev. Cancer* **2022**, *22*, 102−113.
(7) Han, J.; Yoon, J.; Shin, J.; Nam, E.; Qian, T.; Li, Y.; Park, K.; Lee, S. H.; Lim, M. H. Conformational and functional changes of the native neuropeptide somatostatin occur in the presence of copper and amyloid-beta. *Nat. Chem.* **2022**, *14*, 1021−1030.
(8) Huang, D.; Chen, L.; Ji, Q.; Xiang, Y.; Zhou, Q.; Chen, K.; Zhang, X.; Zou, F.; Zhang, X.; Zhao, Z.; Wang, T.; Zheng, G.; Meng, X. Lead aggravates alzheimer's disease pathology via mitochondrial copper accumulation regulated by cox17. *Redox Biol.* **2024**, *69*, 102990.
(9) Bischoff, M. E.; Shamsaei, B.; Yang, J.; Secic, D.; Vemuri, B.; Reisz, J. A.; D'Alessandro, A.; Bartolacci, C.; Adamczak, R.; Schmidt, L.; Wang, J.; Martines, A.; Venkat, J.; Tcheuyap, V. T.; Biesiada, J.; Behrmann, C. A.; Vest, K. E.; Brugarolas, J.; Scaglioni, P. P.; Plas, D. R.; Patra, K. C.; Gulati, S.; Landero Figueroa, J. A.; Meller, J.; Cunningham, J. T.; Czyzyk-Krzeska, M. F. Copper drives remodeling of metabolic state and progression of clear cell renal cell carcinoma. *Cancer Discovery* **2025**, *15*, 401−426.
(10) Chen, L.; Ma, S.; Wu, H.; Zheng, L.; Yi, Y.; Liu, G.; Li, B.; Sun, J.; Du, Y.; Wang, B.; et al. Zonated copper-driven breast cancer progression countered by a copper-depleting nanoagent for immune and metabolic reprogramming. *Adv. Sci.* **2025**, *12* (20), 2412434.

(11) Tsvetkov, P.; Coy, S.; Petrova, B.; Dreishpoon, M.; Verma, A.; Abdusamad, M.; Rossen, J.; Joesch-Cohen, L.; Humeidi, R.; Spangler, R. D.; Eaton, J. K.; Frenkel, E.; Kocak, M.; Corsello, S. M.; Lutsenko, S.; Kanarek, N.; Santagata, S.; Golub, T. R. Copper induces cell death by targeting lipoylated tca cycle proteins. *Science* **2022**, *375*, 1254−1261.
(12) Tsvetkov, P.; Detappe, A.; Cai, K.; Keys, H. R.; Brune, Z.; Ying, W.; Thiru, P.; Reidy, M.; Kugener, G.; Rossen, J.; Kocak, M.; Kory, N.; Tsherniak, A.; Santagata, S.; Whitesell, L.; Ghobrial, I. M.; Markley, J. L.; Lindquist, S.; Golub, T. R. Mitochondrial metabolism promotes adaptation to proteotoxic stress. *Nat. Chem. Biol.* **2019**, *15*, 681−689.
(13) Dreishpoon, M. B.; Bick, N. R.; Petrova, B.; Warui, D. M.; Cameron, A.; Booker, S. J.; Kanarek, N.; Golub, T. R.; Tsvetkov, P. Fdx1 regulates cellular protein lipoylation through direct binding to lias. *J. Biol. Chem.* **2023**, *299*, 105046.
(14) Wang, S.; Liu, X.; Wei, D.; Zhou, H.; Zhu, J.; Yu, Q.; Luo, L.; Dai, X.; Jiang, Y.; Yu, L.; Yang, Y.; Tan, W. Polyvalent aptamer nanodrug conjugates enable efficient tumor cuproptosis therapy through copper overload and glutathione depletion. *J. Am. Chem. Soc.* **2024**, *146*, 30033−30045.
(15) Liu, Y.; Niu, R.; Zhao, H.; Wang, Y.; Song, S.; Zhang, H.; Zhao, Y. Single-site nanozymes with a highly conjugated coordination structure for antitumor immunotherapy via cuproptosis and cascade-enhanced t lymphocyte activity. *J. Am. Chem. Soc.* **2024**, *146*, 3675−3688.
(16) Wang, Y.; Chen, Y.; Zhang, J.; Yang, Y.; Fleishman, J. S.; Wang, Y.; Wang, J.; Chen, J.; Li, Y.; Wang, H. Cuproptosis: A novel therapeutic target for overcoming cancer drug resistance. *Drug Resist. Update* **2024**, *72*, 101018.
(17) Carroll, A. R.; Copp, B. R.; Grkovic, T.; Keyzers, R. A.; Prinsep, M. R. Marine natural products. *Nat. Prod. Rep.* **2025**, *42*, 257−297.
(18) Haque, N.; Parveen, S.; Tang, T.; Wei, J.; Huang, Z. Marine natural products in clinical use. *Mar. Drugs* **2022**, *20*, 528.
(19) Liao, J.-H.; Chien, C.-T.; Wu, H.-Y.; Huang, K.-F.; Wang, I.; Ho, M.-R.; Tu, I.-F.; Lee, I.-M.; Li, W.; Shih, Y.-L.; Wu, C.-Y.; Lukyanov, P. A.; Hsu, S.-T.; Wu, S.-H. A multivalent marine lectin from crenomytilus grayanus possesses anti-cancer activity through recognizing globotriose gb3. *J. Am. Chem. Soc.* **2016**, *138*, 4787−4795.
(20) Krumpe, L. R. H.; Wilson, B. A. P.; Marchand, C.; Sunassee, S. N.; Bermingham, A.; Wang, W.; Price, E.; Guszczynski, T.; Kelley, J. A.; Gustafson, K. R.; Pommier, Y.; Rosengren, K. J.; Schroeder, C. I.; O'Keefe, B. R. Recifin a, initial example of the tyr-lock peptide structural family, is a selective allosteric inhibitor of tyrosyl-DNA phosphodiesterase i. *J. Am. Chem. Soc.* **2020**, *142*, 21178−21188.
(21) An, B.; Yin, F.; de Voogd, N. J.; Chen, X.; Cheng, W.; Lin, W. Chagosendines A − C, New Metal Complexes of Imidazole Alkaloids from the Calcareous Sponge Leucetta chagosensis. *Chem. Biodiversity* **2018**, *15* (2), No. e1700481.
(22) Fu, P. P.; Wang, Q.; Zhang, Q.; Jin, Y.; Liu, J.; Chen, K. X.; Guo, Y. W.; Liu, S. H.; Li, X. W. Bioactivity-driven synthesis of the marine natural product naamidine j and its derivatives as potential tumor immunological agents by inhibiting programmed death-ligand 1. *J. Med. Chem.* **2023**, *66*, 5427−5438.
(23) Gao, C. L.; Song, J. Q.; Yang, Z. N.; Wang, H.; Wu, X. Y.; Shao, C.; Dai, H. X.; Chen, K.; Guo, Y. W.; Pang, T.; Li, X. W. Chemoproteomics of marine natural product naamidine j unveils cse1l as a therapeutic target in acute lung injury. *J. Am. Chem. Soc.* **2024**, *146*, 28384−28397.
(24) Steinbrueck, A.; Sedgwick, A. C.; Brewster, J. T., II; Yan, K. C.; Shang, Y.; Knoll, D. M.; Vargas-Zuniga, G. I.; He, X. P.; Tian, H.; Sessler, J. L. Transition metal chelators, pro-chelators, and ionophores as small molecule cancer chemotherapeutic agents. *Chem. Soc. Rev.* **2020**, *49*, 3726−3747.
(25) Ramchandani, D.; Berisa, M.; Tavarez, D. A.; Li, Z.; Miele, M.; Bai, Y.; Lee, S. B.; Ban, Y.; Dephoure, N.; Hendrickson, R. C.; et al. Copper depletion modulates mitochondrial oxidative phosphorylation to impair triple negative breast cancer metastasis. *Nat. Commun.* **2021**, *12* (1), 7311.
(26) Robert, A.; Liu, Y.; Nguyen, M.; Meunier, B. Regulation of copper and iron homeostasis by metal chelators: A possible chemotherapy for alzheimer's disease. *Acc. Chem. Res.* **2015**, *48*, 1332−1339.
(27) Skrott, Z.; Mistrik, M.; Andersen, K. K.; Friis, S.; Majera, D.; Gursky, J.; Ozdian, T.; Bartkova, J.; Turi, Z.; Moudry, P.; Kraus, M.; Michalova, M.; Vaclavkova, J.; Dzubak, P.; Vrobel, I.; Pouckova, P.; Sedlacek, J.; Miklovicova, A.; Kutt, A.; Li, J.; Mattova, J.; Driessen, C.; Dou, Q. P.; Olsen, J.; Hajduch, M.; Cvek, B.; Deshaies, R. J.; Bartek, J. Alcohol-abuse drug disulfiram targets cancer via p97 segregase adaptor npl4. *Nature* **2017**, *552*, 194−199.
(28) Pan, M.; Zheng, Q.; Yu, Y.; Ai, H.; Xie, Y.; Zeng, X.; Wang, C.; Liu, L.; Zhao, M. Seesaw conformations of npl4 in the human p97 complex and the inhibitory mechanism of a disulfiram derivative. *Nat. Commun.* **2021**, *12* (1), 121.
(29) Chen, X.; Zhang, X.; Chen, J.; Yang, Q.; Yang, L.; Xu, D.; Zhang, P.; Wang, X.; Liu, J. Hinokitiol copper complex inhibits proteasomal deubiquitination and induces paraptosis-like cell death in human cancer cells. *Eur. J. Pharmacol.* **2017**, *815*, 147−155.
(30) Lu, S.; Li, Y.; Yu, Y. Glutathione-scavenging celastrol-cu nanoparticles induce self-amplified cuproptosis for augmented cancer immunotherapy. *Adv. Mater.* **2024**, *36* (35), 2404971.
(31) Zhang, H.; Chen, D.; Ringler, J.; Chen, W.; Cui, Q. C.; Ethier, S. P.; Dou, Q. P.; Wu, G. Disulfiram treatment facilitates phosphoinositide 3-kinase inhibition in human breast cancer cells in vitro and in vivo. *Cancer Res.* **2010**, *70*, 3996−4004.
(32) Kim, J. Y.; Cho, Y.; Oh, E.; Lee, N.; An, H.; Sung, D.; Cho, T. M.; Seo, J. H. Disulfiram targets cancer stem-like properties and the her2/akt signaling pathway in her2-positive breast cancer. *Cancer Lett.* **2016**, *379*, 39−48.
(33) Nagai, M.; Vo, N. H.; Shin Ogawa, L.; Chimmanamada, D.; Inoue, T.; Chu, J.; Beaudette-Zlatanova, B. C.; Lu, R.; Blackman, R. K.; Barsoum, J.; Koya, K.; Wada, Y. The oncology drug elesclomol selectively transports copper to the mitochondria to induce oxidative stress in cancer cells. *Free Radical Biol. Med.* **2012**, *52*, 2142−2150.
(34) Hamza, M.; Wang, S.; Wu, H.; Sun, J.; Du, Y.; Zeng, C.; Liu, Y.; Li, K.; Zhu, X.; Liu, H.; Chen, L.; Zhu, M. Targeting copper homeostasis: Akkermansia-derived omvs co-deliver atox1 sirna and elesclomol for cancer therapy. *Acta Pharm. Sin. B* **2025**, *15*, 2640−2654.
(35) Guo, B.; Yang, F.; Zhang, L.; Zhao, Q.; Wang, W.; Yin, L.; Chen, D.; Wang, M.; Han, S.; Xiao, H.; et al. Cuproptosis Induced by ROS Responsive Nanoparticles with Elesclomol and Copper Combined with αPD-L1 for Enhanced Cancer Immunotherapy. *Adv. Mater.* **2023**, *35* (22), 2212267.
(36) Schulz, V.; Basu, S.; Freibert, S. A.; Webert, H.; Boss, L.; Muhlenhoff, U.; Pierrel, F.; Essen, L. O.; Warui, D. M.; Booker, S. J.; Stehling, O.; Lill, R. Functional spectrum and specificity of mitochondrial ferredoxins fdx1 and fdx2. *Nat. Chem. Biol.* **2023**, *19*, 206−217.
(37) Sheftel, A. D.; Stehling, O.; Pierik, A. J.; Elsasser, H. P.; Muhlenhoff, U.; Webert, H.; Hobler, A.; Hannemann, F.; Bernhardt, R.; Lill, R. Humans possess two mitochondrial ferredoxins, fdx1 and fdx2, with distinct roles in steroidogenesis, heme, and fe/s cluster biosynthesis. *Proc. Natl. Acad. Sci. U. S. A.* **2010**, *107*, 11775−11780.
(38) Sun, L.; Zhang, Y.; Yang, B.; Sun, S.; Zhang, P.; Luo, Z.; Feng, T.; Cui, Z.; Zhu, T.; Li, Y.; et al. Lactylation of METTL16 promotes cuproptosis via m6A-modification on FDX1 mRNA in gastric cancer. *Nat. Commun.* **2023**, *14* (1), 6523.
(39) Ma, J.; Zhang, Y.; Sun, Z.; Guo, H.; Li, X.; Cai, J.; Zhang, M.; Chen, M.; Jiang, J.; Zhang, L. Lncrna pvt1 promotes cuproptosis through transcriptional activation of fdx1 in colorectal cancer. *Redox Biol.* **2025**, *85*, 103722.
(40) Zulkifli, M.; Spelbring, A. N.; Zhang, Y.; Soma, S.; Chen, S.; Li, L.; Le, T.; Shanbhag, V.; Petris, M. J.; Chen, T.-Y.; et al. Fdx1-dependent and independent mechanisms of elesclomol-mediated intracellular copper delivery. *Proc. Natl. Acad. Sci. U. S. A.* **2023**, *120* (10), No. e2216722120.

(41) Sun, H.; Zou, Y.; Chen, Z.; He, Y.; Ye, K.; Liu, H.; Qiu, L.; Zhang, Y.; Mai, Y.; Chen, X.; et al. Nanodrug-engineered exosomes achieve a jointly dual-pathway inhibition on cuproptosis. *Adv. Sci.* **2024**, *12* (4), 2413408.
(42) Sun, Z.; Xu, H.; Lu, G.; Yang, C.; Gao, X.; Zhang, J.; Liu, X.; Chen, Y.; Wang, K.; Guo, J.; et al. Akt1 phosphorylates fdx1 to promote cuproptosis resistance in triple-negative breast cancer. *Adv. Sci.* **2025**, *12* (17), 2408106.
(43) Wang, W.; Lu, K.; Jiang, X.; Wei, Q.; Zhu, L.; Wang, X.; Jin, H.; Feng, L. Ferroptosis inducers enhanced cuproptosis induced by copper ionophores in primary liver cancer. *J. Exp. Clin. Cancer Res.* **2023**, *42* (1), 142.

https://doi.org/10.1021/jacs.5c07917
J. Am. Chem. Soc. 2025, 147, 37089−37103